

Impact of a Warm Dark Matter late-time velocity dispersion on large-scale structures

Patrick Valageas

Institut de Physique Théorique,

CEA, IPhT, F-91191 Gif-sur-Yvette, Cédex, France

CNRS, URA 2306, F-91191 Gif-sur-Yvette, Cédex, France

(Dated: February 25, 2024)

We investigate whether the late-time (at $z \leq 100$) velocity dispersion expected in Warm Dark Matter scenarios could have some effect on the cosmic web (i.e., outside of virialized halos). We consider effective hydrodynamical equations, with a pressurelike term that agrees at the linear level with the analysis of the Vlasov equation. Then, using analytical methods, based on perturbative expansions and the spherical dynamics, we investigate the impact of this term for a 1keV dark matter particle. We find that the late-time velocity dispersion has a negligible effect on the power spectrum on perturbative scales and on the halo mass function. However, it has a significant impact on the probability distribution function of the density contrast at $z \sim 3$ on scales smaller than $0.1h^{-1}\text{Mpc}$, which correspond to Lyman- α clouds. Finally, we note that numerical simulations should start at $z_i \geq 100$ rather than $z_i \leq 50$ to avoid underestimating gravitational clustering at low redshifts.

PACS numbers: 98.80.-k, 95.35.+d

I. INTRODUCTION

In the standard cosmological Λ cold dark matter (ΛCDM) scenario, most of the matter content of the Universe is made of CDM particles, which are cold and collisionless. This means that they have a negligible velocity dispersion during the matter-dominated era and density fluctuations on almost all scales (except very small scales at early times) grow through gravitational instability. This leads to a hierarchical scenario for the formation of large-scale structures, as the amplitude of density fluctuations at early time (e.g., at the beginning of the matter-dominated era) is larger on smaller scales. Then, small scales turn nonlinear first and merge to build increasingly large and massive structures as larger scales become nonlinear in the course of time [1]. This scenario (with an extra dark energy component or cosmological constant) is in good agreement with a large variety of cosmological observations, such as the cosmic microwave background (CMB) [2] and galaxy surveys [3].

However, this CDM model may disagree from observations on small scales (below the size of galaxies). Thus, CDM simulations typically predict too many satellite galaxies around Milky-Way-sized central galaxies as compared with observations [4–6]. They also predict power-law density profiles, $\rho \sim r^{-1}$, in the center of virialized halos [7], whereas dark-matter-dominated dwarf galaxies [8] and some disk galaxies [9] exhibit flat density cores. This is the so-called “core-cusp problem” [10].

One possible solution to these small-scale problems is a warm dark matter (WDM) scenario, with dark matter particles of a mass on the order of 1keV. This intermediate case between the “cold” and “hot” dark matter scenarios provides a non-negligible velocity dispersion and a significant free-streaming that erases density fluctuations on small scales (mostly during the period where the particles are relativistic). This helps to cure the small-scale problems of the CDM scenario, while being

indistinguishable from CDM on large scales, which preserves its good agreement with large-scale observations such as the CMB and galaxy surveys [11–14]. This favors a mass on the order of 1keV [15, 16]. For larger masses we recover the CDM scenario and for smaller masses we recover the hot dark matter scenario, where structure formation begins too late (in particular, this is ruled out by the Gunn-Peterson bound [17]: quasar spectra show that the Universe must have been reionized before $z \sim 6$, which requires galaxy formation by this time). Similar lower bounds on m are also obtained from the observed velocity dispersion of dwarfs galaxies and from the Lyman- α forest [18–21].

We must note that these small-scale problems may also be cured by the physics of the baryonic component, within the CDM scenario. For instance, reionization of the intergalactic medium [22, 23] or feedback from stars and supernovae [24] suppress star formation in small satellite halos. Only a small fraction of the low-mass dark matter satellites would then shine in the sky and appear in galaxy surveys. This would reconcile the observed abundance with the CDM prediction but there remains some discrepancy for the shape of the satellite luminosity function [25]. Supernovae explosions may also transform a cusp density profile into a cored one, within small dark matter halos [26–28]. However, it is a difficult task to check that such models can explain galaxy properties from massive to dwarf galaxies and from $z = 0$ to higher redshifts [29].

Therefore, WDM scenarios remain interesting alternatives to CDM that are still being investigated in many works. As recalled above, a particle mass on the order of 1–10keV is a good candidate and it may correspond, for instance, to sterile neutrinos [30–36] or to gravitinos [37, 38]. At early times and on large scales, the formation of large-scale structures within WDM scenarios is studied through the linearized Vlasov equation [39–43]. At low redshift and on small scales, the nonlinear regime of

gravitational clustering is investigated through numerical simulations [11, 44] and halo models based on such simulations [45, 46]. In practice, one often uses the same N-body codes as for CDM scenarios and the only difference comes from the density power spectrum that is set at the initial redshift z_i of the simulations. This means that one takes into account the high- k cutoff due to free-streaming during the relativistic era but neglects the nonzero velocity dispersion at low redshifts, $z \leq z_i$. This is legitimate because the relative importance of this late-time velocity dispersion decreases with time and the main difference between the CDM and WDM scenarios with respect to large-scale structures arises from the high- k cutoff of the power spectrum built during the relativistic regime. Nevertheless, it would be interesting to have a quantitative check of this approximation. This is the goal of this paper, where we obtain a quantitative estimate of the impact of the late-time WDM velocity dispersion on the formation of large-scale structures. We also estimate the sensitivity of the gravitational clustering measured at low redshift on the initial redshift z_i of the simulations.

Here we do not consider the inner regions of virialized halos, where the finite velocity dispersion can have important effects because of Liouville theorem. Indeed, this implies an upper bound on the coarse-grained phase-space distribution function [47], which can lead to cored density profiles instead of cusps [48] (but the behavior in central regions remains difficult to predict [49]). In contrast, we consider the cosmic web, that is, moderate density fluctuations or large scales, as well as the halo mass function itself. Then, using perturbative methods or the spherical dynamics, we compare such statistics (the power spectrum on large perturbative scales, the halo mass function, and the probability distribution of the density contrast) between the CDM and WDM scenarios, where we neglect or take into account the late-time WDM velocity dispersion. To simplify the analysis and to go beyond the linear regime, we use effective equations of motion similar to standard hydrodynamics. They involve a simplified pressurelike term in the Euler equation, associated with the late-time velocity dispersion, that is chosen so as to agree with results from the Vlasov equation at linear order. This should be sufficient for our goal, which is only to estimate the order of magnitude of the impact of this late-time WDM velocity dispersion. Thus, our study is complementary to Ref.[41] who investigates the effects of the velocity dispersion at low redshift through the linearized Vlasov equation. Our approach is not exact, because we use a fluid approximation, but it allows us to consider nonlinear density fluctuations. In particular, our goal is not to study in accurate details a specific WDM model but to investigate the generic impact of a late-time velocity dispersion on the cosmic web. After describing these effective equations of motion and our approach in Sec. II, we present our results for a 1keV dark matter particle in Sec. III. We also consider the impact of the choice of initial redshift in numerical simulations in Sec. IV and we conclude in

Sec. V.

II. EQUATIONS OF MOTION

A. Effective Euler equation

During the matter-dominated era, on scales much smaller than the Hubble radius and for nonrelativistic particles, the evolution of the dark matter density perturbations is governed by the nonrelativistic Boltzmann-Vlasov equation [1],

$$\frac{\partial f}{\partial \tau} + \frac{\mathbf{p}}{ma} \cdot \frac{\partial f}{\partial \mathbf{x}} - ma \frac{\partial \Phi}{\partial \mathbf{x}} \cdot \frac{\partial f}{\partial \mathbf{p}} = 0, \quad (1)$$

$$\Delta \Phi = \frac{4\pi G m}{a} \left(\int d\mathbf{p} f - \bar{n} \right). \quad (2)$$

Here τ is the conformal time, $a(t)$ the scale-factor, \mathbf{x} and \mathbf{p} are comoving coordinate and momentum, m is the mass of the particles, \bar{n} the mean dark matter number density, and $f(\mathbf{x}, \mathbf{p}, \tau)$ the phase-space distribution function. Because the gravitational potential Φ depends on the dark matter density fluctuations (here we neglected the contribution from baryons, or, more precisely, we neglect the difference between baryons and dark matter), the Vlasov equation (1) is nonlinear over f . Then, one usually linearizes the system (1)-(2) to study the evolution of the dark matter perturbations [39, 40].

The phase-space distribution $f(\mathbf{x}, \mathbf{p}, \tau)$ includes the distribution of velocities of the dark matter particles at any point in space. However, for observational purposes one is mostly interested in the density and peculiar velocity fields, which are the lowest-order moments of f ,

$$\int d\mathbf{p} f = \frac{\rho}{m}, \quad \int d\mathbf{p} \mathbf{p} f = a\rho\mathbf{v}. \quad (3)$$

By taking successive moments over \mathbf{p} of the Vlasov equation (1) one obtains an infinite hierarchy of equations that no longer depend on the velocity coordinate [1, 50]. However, contrary to the case of collisional fluids, this hierarchy cannot be closed by writing the second-order moment (the velocity dispersion) as a pressure that obeys a definite equation of state. In the case of cold dark matter, this hierarchy can still be closed by neglecting the velocity dispersion (whence the name ‘‘cold’’) and one is left with only two fields, the density $\rho(\mathbf{x}, \tau)$ and the mean peculiar velocity $\mathbf{v}(\mathbf{x}, \tau)$. In the case of warm dark matter, the velocity dispersion cannot be neglected at high redshift and one must work with the Vlasov equation. This large velocity dispersion leads to a significant free streaming that damps the early time density power spectrum at high k , as compared with CDM, because particles can escape from small potential wells [11]. This is very efficient at early times, when the particles are still relativistic. Therefore, the damping is greater for particles of smaller mass m , which become nonrelativistic

later. Afterwards, because the typical comoving velocity dispersion decreases with time because of the Hubble expansion, these effects become less important on large scales. (However, because of Liouville theorem, the finite velocity dispersion, which leads to a finite value for the initial phase-space density f —as opposed to the cold case where it would be a Dirac distribution—leads to an upper bound for the coarse-grained phase-space distribution [47]. This can have a significant effect on the matter distribution on small scales, within collapsed halos, even today [48].)

To go beyond the linear regime, one usually runs numerical simulations to investigate the formation of the cosmic web and collapsed halos. In practice, one often uses the same codes as for CDM [11, 44, 46, 51] and the only difference is encapsulated in the initial density power spectrum set at the initial redshift z_i of the simulation (i.e., the high- k cutoff due to early time free streaming). Sometimes, in order to mimic the effect of the upper bound for the coarse-grained phase-space distribution, one adds an initial white-noise velocity component to the particles of the simulation [52–54]. However, this is not truly equivalent to the full phase-space distribution $f(\mathbf{x}, \mathbf{p}, \tau)$ because the “particles” used in the simulations are actually “macroparticles”, which model large clumps of matter, rather than the physical dark matter particles.

Our goal in this paper is to estimate the impact of a late-time WDM velocity dispersion on large-scale gravitational clustering. As explained above, within a hydrodynamical approach, one cannot truly close the hierarchy of equations obeyed by the successive moments of the phase-space distribution. However, because the fluid equations are much easier to follow beyond the linear level than the Vlasov equation and we only look for an order-of-magnitude estimate in this simple study, we will use a simple closure inspired from linear theory. As shown for instance in [39, 40], in the matter dominated era, one can derive from the linearized Vlasov equation an evolution equation for the matter density contrast of the form

$$\frac{\partial^2 \tilde{\delta}}{\partial \tau^2} + \mathcal{H} \frac{\partial \tilde{\delta}}{\partial \tau} - \left(\frac{3}{2} \Omega_m \mathcal{H}^2 - k^2 c_s^2 \right) \tilde{\delta} = S[\tilde{\delta}, \tau], \quad (4)$$

where $\Omega_m(\tau)$ is the matter cosmological parameter, $\mathcal{H} = \dot{a}$ is the conformal expansion rate, and we denote with a tilde Fourier-space fields such as $\tilde{\delta}(\mathbf{k}, \tau)$. This corresponds to Eq.(2.85) in [39], with a different time variable. Equation (4) becomes identical to the standard equation for the linear density modes in CDM scenarios when we set $c_s = 0$ and $S = 0$.

The new term in the left-hand side is similar to a pressure term (at the linear level), and c_s would be the comoving sound speed. The comoving Jeans wave number k_J would thus correspond to the comoving free-streaming wave number k_{fs} , with

$$k_{\text{fs}}^2 = \frac{3\Omega_m \mathcal{H}^2}{2c_s^2}. \quad (5)$$

However, this is only a formal analogy because there is no true pressure as we consider a collisionless fluid. This term arises from the nonzero velocity dispersion and its evolution with time is set by the comoving free-streaming wave number (5) rather than by a thermodynamical equation of state. At this linear level, $k_{\text{fs}}(\tau)$ is obtained from the analysis of the linearized Vlasov equation. This yields [39, 40]

$$k_{\text{fs}}(\tau) = k_{\text{fs}}(\tau_{\text{eq}}) \sqrt{\frac{a}{a_{\text{eq}}}}, \quad (6)$$

where a_{eq} is the scale factor at the matter-radiation equality, $a_{\text{eq}} = 1/(1 + z_{\text{eq}})$, with $z_{\text{eq}} \simeq 3050$, and

$$k_{\text{fs}}(\tau_{\text{eq}}) \simeq \frac{11.17}{\sqrt{\bar{y}^2}} \left(\frac{m}{1 \text{keV}} \right) \left(\frac{g_d}{2} \right)^{1/2} \text{Mpc}^{-1}, \quad (7)$$

where $\bar{y}^2 \sim 10$ depends on the shape of the initial velocity distribution, g_d is the effective number of relativistic degrees of freedom at decoupling, and m is the mass of the dark matter particles.

The new source term in the right-hand side of Eq.(4) can be decomposed as a memory term S_{NB} (i.e., an integral over past times) and an inhomogeneous term S_{B} (i.e., an integral over the “initial” condition at matter-radiation equality); see [39, 40]. The nonlocal term S_{NB} decreases as $(k/k_{\text{fs}})^4$ at low k , hence, it is subdominant on large scales as compared with the new term in the left-hand side. The inhomogeneous term only decreases as k^2 , but its relative importance decays with time, as compared with the growing mode associated with the left-hand side.

In this paper, we neglect the source term S , and we investigate the equations of motion

$$\frac{\partial \delta}{\partial \tau} + \nabla \cdot [(1 + \delta)\mathbf{v}] = 0, \quad (8)$$

$$\frac{\partial \mathbf{v}}{\partial \tau} + \mathcal{H}\mathbf{v} + (\mathbf{v} \cdot \nabla)\mathbf{v} = -\nabla\Phi - \frac{c_s^2 \nabla \rho}{\bar{\rho}}, \quad (9)$$

where the gravitational potential is given by the Poisson equation (2), which also reads as

$$\nabla^2 \Phi = \frac{3}{2} \Omega_m \mathcal{H}^2 \delta. \quad (10)$$

Equation (8) is the usual continuity equation, which is exact when \mathbf{v} is the mean peculiar velocity as defined by Eq.(3). Equation (9) is the Euler equation, which only differs from the CDM case by the last term. This equation is not exact, because as explained above this last term should be written in terms of the nonzero velocity dispersion, which obeys a third evolution equation that involves the third-order velocity moment, and so on. The expression (9) is the simplest closure of this hierarchy that agrees with the linear theory (4) (where we neglect the source term S). In a fluid analogy, where c_s would be a uniform isothermal sound speed, this term would

be modified beyond linear order because it would read as $(\nabla\rho)/\rho$ instead of $(\nabla\rho)/\bar{\rho}$. However, because this analogy is not exact (and does not need to be strictly followed) and to simplify the analysis, we keep the linear term of Eq.(9). This also ensures that we always mimic the slowdown of gravitational collapse on small scales as compared with CDM. (In contrast, a truncation at a finite order over δ of $\nabla\delta/(1+\delta)$ is not very well behaved. For instance, depending on whether the truncation order p is odd or even a term $(-1)^{p-1}\delta^{p-1}\nabla\delta$ either slows down or speeds up the dynamics of overdense regions).

B. Setup

The closure (9) should be sufficient for our purpose, which is not to obtain the most accurate predictions for large-scale statistics but to estimate the impact of a late-time velocity dispersion. Equations (8)-(9) read in Fourier space as

$$\frac{\partial\tilde{\delta}}{\partial\tau}(\mathbf{k},\tau) + \tilde{\theta}(\mathbf{k},\tau) = - \int d\mathbf{k}_1 d\mathbf{k}_2 \delta_D(\mathbf{k}_1 + \mathbf{k}_2 - \mathbf{k}) \times \alpha(\mathbf{k}_1, \mathbf{k}_2) \tilde{\theta}(\mathbf{k}_1, \tau) \tilde{\delta}(\mathbf{k}_2, \tau), \quad (11)$$

$$\frac{\partial\tilde{\theta}}{\partial\tau}(\mathbf{k},\tau) + \mathcal{H}\tilde{\theta}(\mathbf{k},\tau) + \frac{3\Omega_m}{2}\mathcal{H}^2[1 + \epsilon(k,\tau)]\tilde{\delta}(\mathbf{k},\tau) = - \int d\mathbf{k}_1 d\mathbf{k}_2 \delta_D(\mathbf{k}_1 + \mathbf{k}_2 - \mathbf{k}) \beta(\mathbf{k}_1, \mathbf{k}_2) \tilde{\theta}(\mathbf{k}_1, \tau) \tilde{\theta}(\mathbf{k}_2, \tau), \quad (12)$$

where we introduced the velocity divergence, $\theta = \nabla \cdot \mathbf{v}$. The usual kernels α and β are given by

$$\alpha(\mathbf{k}_1, \mathbf{k}_2) = \frac{(\mathbf{k}_1 + \mathbf{k}_2) \cdot \mathbf{k}_1}{k_1^2}, \beta(\mathbf{k}_1, \mathbf{k}_2) = \frac{|\mathbf{k}_1 + \mathbf{k}_2|^2 (\mathbf{k}_1 \cdot \mathbf{k}_2)}{2k_1^2 k_2^2}, \quad (13)$$

and the factor $\epsilon(k, \tau)$ writes as

$$\epsilon(k, \tau) = - \frac{k^2}{k_{\text{fs}}(\tau)^2}. \quad (14)$$

Combining Eqs.(11) and (12) at linear order, we recover the left-hand side of Eq.(4). The equations of motion (11)-(12) have the same form as those studied in [55] in the context of modified gravity models, but with a different kernel $\epsilon(k, \tau)$. Therefore, we can use the same methods as in [55] to investigate large-scale structure formation.

To fully define our system, we must specify our initial conditions. Following [18], we write the linear density power spectrum today in terms of the reference CDM power spectrum as

$$P_{L,\text{WDM}}(k, z=0) = P_{L,\text{CDM}}(k, z=0) T(k)^2, \quad (15)$$

with

$$T(k) = [1 + (\alpha k)^{2\nu}]^{-5/\nu}, \quad (16)$$

with $\nu = 1.12$ and

$$\alpha = 0.049 \left(\frac{m}{1\text{keV}}\right)^{-1.11} \left(\frac{\Omega_m}{0.25}\right)^{0.11} \left(\frac{h}{0.7}\right)^{1.22} h^{-1} \text{Mpc}. \quad (17)$$

The high- k cutoff (16) is due to free streaming in the relativistic regime, which damps the growth of small-scale clustering as compared with CDM.

Then, in a manner similar to what is done in numerical simulations, we choose an ‘‘initial’’ redshift $z_i = 100$, and we write the initial power spectrum as $P_L(k, z_i) = [D_+(z_i)/D_+(0)]P_{\text{WDM}}(k, 0)$, where $D_+(z)$ is the CDM linear growing mode, which is independent of k (it is the growing solution of Eq.(4) with $c_s = 0$ and $S = 0$). Next, for a given initial redshift z_i , we compute the subsequent formation of large-scale structure defined by the equations of motion (11)-(12) with either $\epsilon \neq 0$ (i.e., taking into account the late-time velocity dispersion through the last term in Eq.(9)) or $\epsilon = 0$ (i.e., neglecting this late-time velocity dispersion), starting with the same initial WDM power spectrum (15). Comparing these two results we obtain an estimate of the impact of the nonzero velocity dispersion at low redshifts, below z_i . Comparing with a pure CDM scenario, with the initial power spectrum P_{CDM} , we compare this effect with the damping due to the initial high- k cutoff (16), which mostly arises from the relativistic era. This will allow us to check whether the late-time dark matter velocity dispersion can be neglected on large scales (outside of collapsed objects where the upper bound associated with Liouville theorem may be important). This is often the assumption used in numerical simulations, where the system is modeled with the same codes as for CDM and the only difference lies in the initial condition at redshift z_i , that is, in the damping (16) of the initial power spectrum [11, 44, 46, 51].

In some cases, one adds to the macroparticles used in the N-body simulations an additional initial random velocity, v_{rms} , drawn from the thermal distribution $f(v)$ of the WDM particles [52–54]. However, this is not fully legitimate because these macroparticles have a much larger mass ($\sim 10^5 M_\odot$) than the WDM particles and a clump of this mass of many elementary dark matter particles would have a much smaller (almost zero) mean velocity. In fact, setting such initial conditions at $z_i = 100$ leads to spurious power at high k in the power spectrum measured at later times (starting at $z_i = 40$ appears to avoid this problem because v_{rms} is smaller) [52]. This can be understood from the fact that adding these random velocities is equivalent to model a CDM scenario, with the damped power spectrum (15), to which is added a k^2 high- k tail associated with the random velocity component. Indeed, this adds a white-noise component to the initial velocity power spectrum, which corresponds to a k^2 tail for the density power spectrum (when we decompose over growing and decaying modes). On the other hand, these additional random velocities can be seen as an effective tool to build an upper bound on the phase-space distribution function and to investigate the formation of cored profiles associated with Liouville theorem

[56]. However, this shows that it is not easy to include the WDM velocity dispersion in numerical simulations in a realistic fashion. This is another motivation for the analytic study presented in this paper.

In the following, as in [44], for numerical computations we adopt a background cosmology that is consistent with WMAP7 [2], $\Omega_m = 0.2726$, $\Omega_\Lambda = 0.7274$, $\Omega_b = 0.046$, $h = 0.704$, $n_s = 0.963$, and $\sigma_8 = 0.809$.

We focus on the case of a 1 keV dark matter particle, and we take $\bar{y}^2 = 12.939$ as for thermal fermions (or sterile neutrinos produced via the Dodelson-Widrow [30] nonresonant mixing mechanism) and $g_d = 10.75$ [18, 40]. This gives $k_{\text{fs}}(\tau_{\text{eq}}) \simeq 10h\text{Mpc}^{-1}$. The comoving free-streaming distance, traveled by particles since t_{eq} because of thermal velocities,

$$\lambda_{\text{fs}}(t) = \int_{t_{\text{eq}}}^t \frac{dt'}{a(t')} c_s(t'), \quad (18)$$

converges at late times to [39]

$$t \gg t_{\text{eq}} : \lambda_{\text{fs}} \simeq \frac{\sqrt{6}}{k_{\text{fs}}(\tau_{\text{eq}})} \simeq 0.24h^{-1}\text{Mpc} \quad (19)$$

This gives the scale below which the velocity dispersion of the warm dark matter has a strong effect.

III. RESULTS

A. Matter density power spectrum

Since the equations of motion (11)-(12) have the same form as those studied in [55] in the context of modified gravity models (but with a different kernel $\epsilon(k, \tau)$) we use the same methods as in [55] for our numerical computations. We refer the reader to [55] for a description of our analytical methods.

Because of the explicit dependence on k introduced in the left-hand side of the Euler equation (12) by the factor $\epsilon(k, \tau)$, the linear growing and decaying modes of the density contrast now depend on k . As explained above, they also satisfy Eq.(4), with $S = 0$, where the dependence on k is explicit. This pressurelike term, $-k^2 c_s^2$, slows down the growth of density perturbations at high k . For $k > k_{\text{fs}}$, which plays the role of a Jeans wave number, density perturbations would no longer grow but oscillate. We show in the lower panel of Fig. 1 the linear growing mode $D_+(k, \tau)$ as a function of the wave number. (We normalize all linear growing modes to the CDM mode at the initial redshift z_i .) We clearly see the decrease of the growing mode above $k \sim 1/\lambda_{\text{fs}} \sim 4h\text{Mpc}^{-1}$. For comparison, we also plot in the upper panel the ratio $P_{L,\text{WDM}}/P_{L,\text{CDM}} = T(k)^2$ of the linear WDM to CDM power spectra, from Eq.(15). All curves deviate from the CDM prediction at about the same wave number, but, as expected, the damping of the linear power spectrum is stronger than the damping of the late-time

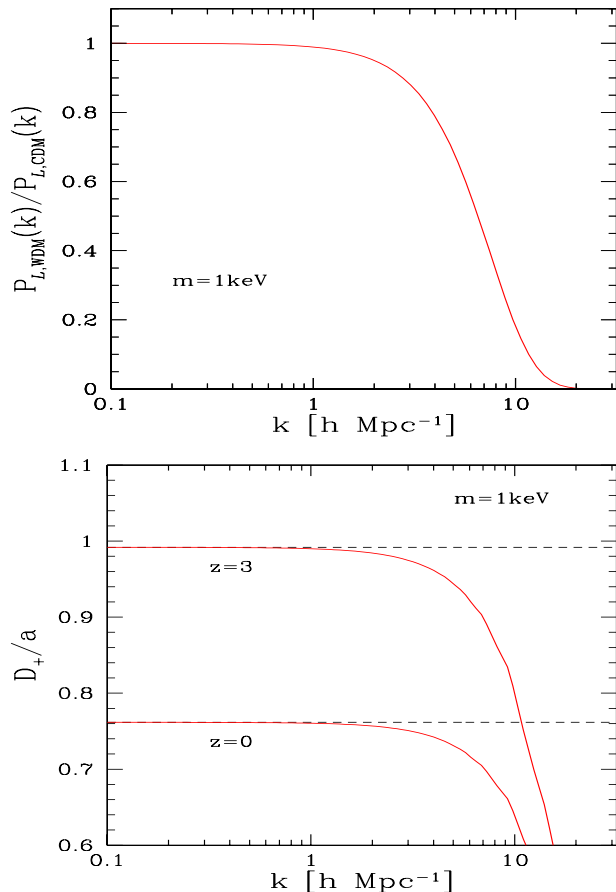


FIG. 1: *Upper panel*: ratio $T(k)^2 = P_{L,\text{WDM}}/P_{L,\text{CDM}}$ of the linear WDM and CDM power spectra at $z = 0$, from Eq.(15). *Lower panel*: linear growing mode $D_+(k, \tau)$ normalized to the scale factor $a(\tau)$ as a function of the wave number. We show our results at $z = 0$ and $z = 3$ for the CDM case (black dashed lines) and the WDM case (red solid lines) with $m = 1\text{ keV}$.

linear growing mode. Indeed, the damping of the linear power spectrum shown in the upper panel is mostly due to early-time effects, when the dark matter particles were still relativistic. In contrast, by definition of our initial conditions at $z_i = 100$, the damping found in the lower panel is a late-time effect at $z < z_i$, due to the small nonzero velocity dispersion. This effect declines with time as the comoving wave number $k_{\text{fs}}(\tau)$ grows as \sqrt{a} from Eq.(6). However, it is not zero and we will estimate in the following the magnitude of this late-time effect.

Next, we consider the nonlinear density power spectrum in the perturbative regime in Figs. 2 and 3. We compare the results associated with the reference ΛCDM scenario, the WDM scenario with $c_s = 0$ (i.e., the only difference from CDM arises from the initial power (15)), and the WDM scenario with $c_s \neq 0$ (i.e., the difference from CDM arises from both the initial power (15) and the late-time velocity-dispersion). To emphasize the

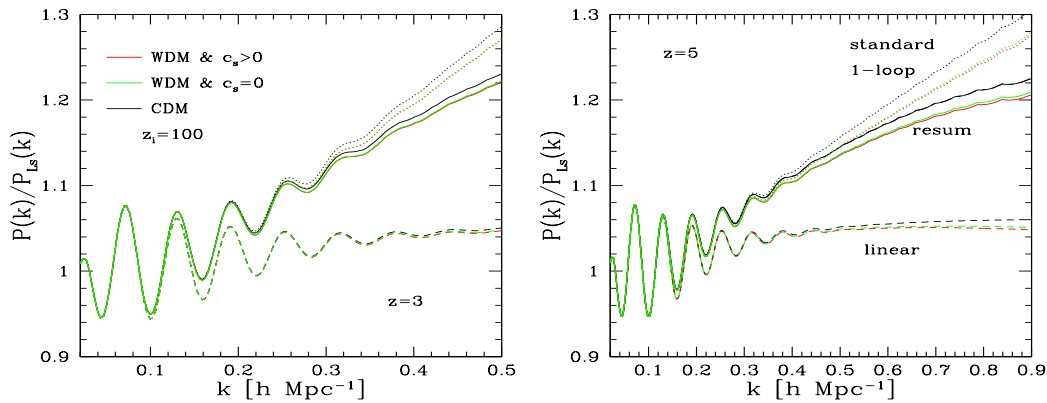


FIG. 2: Ratio of the power spectrum $P(k)$ to a smooth Λ CDM linear power spectrum $P_{L_s}(k)$ without baryonic oscillations, from [57]. We plot the linear power (lower group of dashed lines), the nonlinear one-loop “steepest descent” resummation (middle group of solid lines), and the “standard” 1-loop result (upper group of dotted lines). In each case, we show our results for the reference CDM scenario (slightly upper black lines), the WDM scenario with $c_s = 0$ (middle green lines) and with $c_s \neq 0$ (slightly lower red lines).

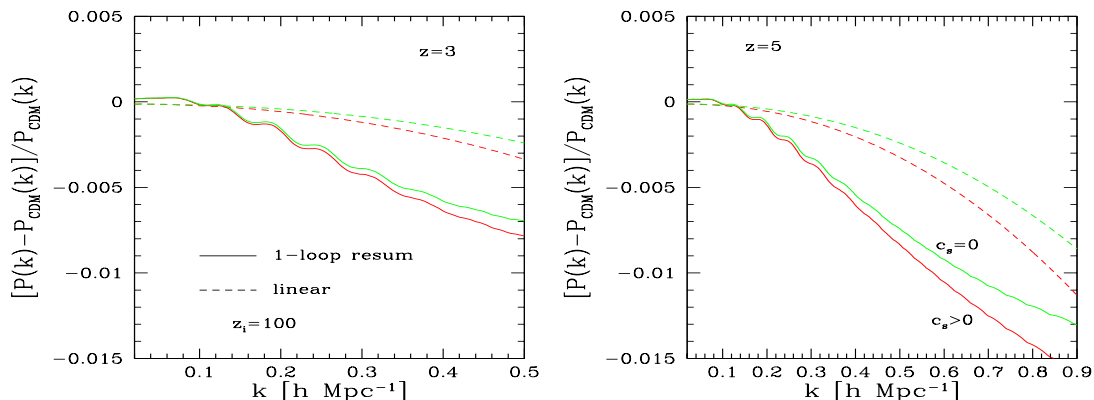


FIG. 3: Relative deviation of the power spectrum from the CDM reference, in terms of the linear power spectra ($\Delta P_L/P_L$, upper group of dashed lines), and of the nonlinear power spectra ($\Delta P/P$, lower group of solid lines) obtained from the one-loop “steepest descent” resummation. In each case, we show our results for the WDM scenarios with $c_s = 0$ (slightly upper green lines) and with $c_s \neq 0$ (slightly lower red lines).

difference between various curves, we plot the ratios of our results by a common reference linear power spectrum without baryonic oscillations, from [57], in Fig. 2. We plot both the “standard” one-loop perturbative result [58] and the “steepest-descent resummation” [59–61], which agrees with the standard result up to one loop and contains a partial resummation of higher-order terms [76].

We recover the suppression of the nonlinear power spectrum due to the high- k cutoff (16) [46]. As in the usual CDM case, we can see that the nonlinear dynamics amplifies the power spectrum while erasing some of the baryonic oscillations. The difference between the “standard” and the “resummed” perturbative predictions is similar to the one obtained in the CDM scenario, and it is larger than the difference between the CDM and WDM

results. This means that on these scales, the standard perturbation theory is not accurate enough to describe the deviations between the CDM and WDM predictions (for $m \geq 1\text{keV}$), which are on the order of 1% as seen in Fig. 3.

On the other hand, we can see that nonlinear contributions amplify these deviations, as compared with the linear power spectra. This is more clearly seen in Fig. 3, where we plot the relative deviations from the reference linear and nonlinear CDM power spectra. The comparison of the curves obtained with $c_s = 0$ and $c_s \neq 0$ shows that most of the damping with respect to the CDM case is due to the cutoff (16) of the initial power spectrum. The late-time velocity dispersion only slightly amplifies the damping on these scales. Thus, for practical purposes, this late-time effect may be neglected. This jus-

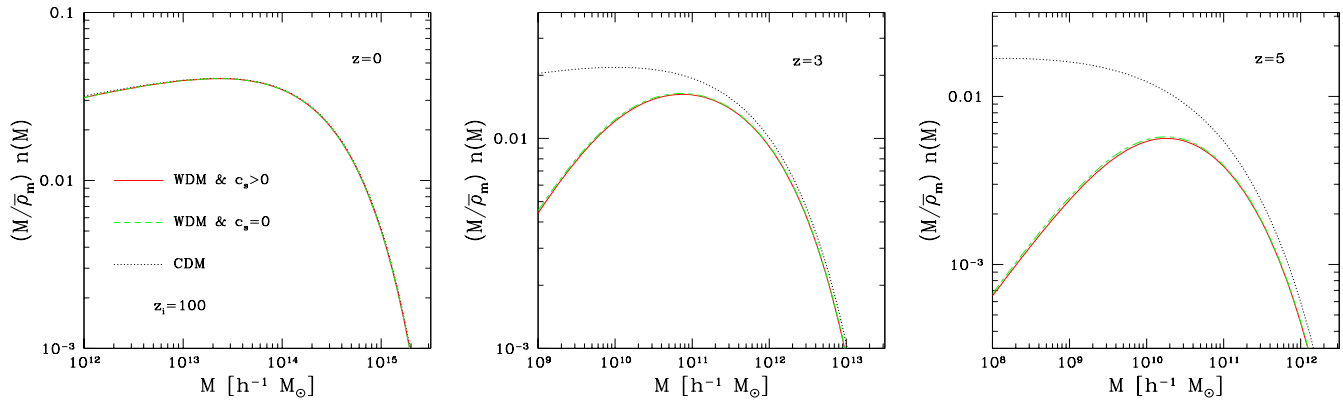


FIG. 4: Halo mass functions for the reference CDM scenario (black dotted lines), the WDM scenarios with $c_s = 0$ (green dashed lines), and with $c_s \neq 0$ (red solid lines).

tifies the use of N-body simulations, initially built for CDM, to study gravitational clustering on these scales [44, 46]. However, for $m \geq 1\text{keV}$, the difference from the CDM power is not larger than 1.5% on these scales. This means that, as expected, most of the constraints that can be set from observations on the WDM scenario arise from smaller scales. However, because these smaller scales are also more difficult to predict (since they are deeper in the nonlinear or nonperturbative regime), it is interesting to check the signal that can be expected on the larger perturbative scales shown in Figs. 2 and 3, which are better controlled since they can be described by systematic perturbative schemes.

B. Halo mass function

Another key statistic of large-scale structures is the mass function of collapsed halos. As in [55] we define halos by a nonlinear density contrast of 200. Then, we obtain the halo mass function from the spherical dynamics, using the Press-Schechter scaling variable ν [62],

$$n(M) \frac{dM}{M} = \frac{\bar{\rho}_m}{M} f(\nu) \frac{d\nu}{\nu}, \quad (20)$$

with

$$\nu = \frac{\mathcal{F}_q^{-1}(200)}{\sigma_q}, \quad (21)$$

and the scaling function $f(\nu)$ from [63]

$$f(\nu) = 0.502 [(0.6\nu)^{2.5} + (0.62\nu)^{0.5}] e^{-\nu^2/2}, \quad (22)$$

which has been fitted to ΛCDM numerical simulations. This ensures that the halo mass function is always normalized to unity and obeys the large-mass tail $n(M) \sim e^{-\nu^2/2}$ for any spherical-collapse mapping \mathcal{F}_q . We obtain the spherical dynamics associated with the equations of

motion (11)-(12) as in [55]. This provides the spherical-collapse mapping, $\delta_{Lq} \mapsto \delta_x = \mathcal{F}_q(\delta_{Lq})$, from the linear density contrast on the Lagrangian radius q to the non-linear density contrast on the Eulerian radius x .

We show our results in Fig. 4. The low-mass tail should be considered with caution because its exponent may depend on the shape of the linear power spectrum and be different from the CDM case. Thus, numerical simulations suggest that a simple recipe of the form (20), which involves a scaling function $f(\nu)$ fitted to CDM simulations, overestimates the low-mass tail in WDM scenarios [44]. In contrast, the large-mass tail is better controlled because it is governed by spherically symmetric saddle points (and it does not involve the multiple mergers that affect the low-mass tail).

As is well known, the WDM scenario leads to a much smaller halo mass function at low masses than in the CDM case, because of the lack of power on small scales [11, 44, 46]. For our purposes, Fig. 4 shows that the impact of the late-time velocity dispersion on the halo mass function at $z \leq 5$ can be neglected for $m \geq 1\text{keV}$. Indeed, the difference between the two WDM curves associated with either $c_s \neq 0$ or $c_s = 0$ at $z \leq z_i$ is much smaller than the deviation from the CDM reference. It is also smaller than the accuracy of halo mass functions that can be obtained from phenomenological models or numerical simulations. Again, this means that standard N-body codes can be used to predict the halo mass function for WDM scenarios (with $m \geq 1\text{keV}$).

This agrees with results from [64], which also model the velocity dispersion as an effective pressure term and compute the delay of halo collapse by this hydrodynamical-like pressure for a spherical dynamics. They also find that the initial cutoff of the linear power spectrum plays a greater role than halo dynamics, but the latter becomes significant at very low mass and high redshift (the late-time velocity dispersion has a very small effect below $z < 40$).

Figure 4 can be compared with Fig. 7 of [65], which

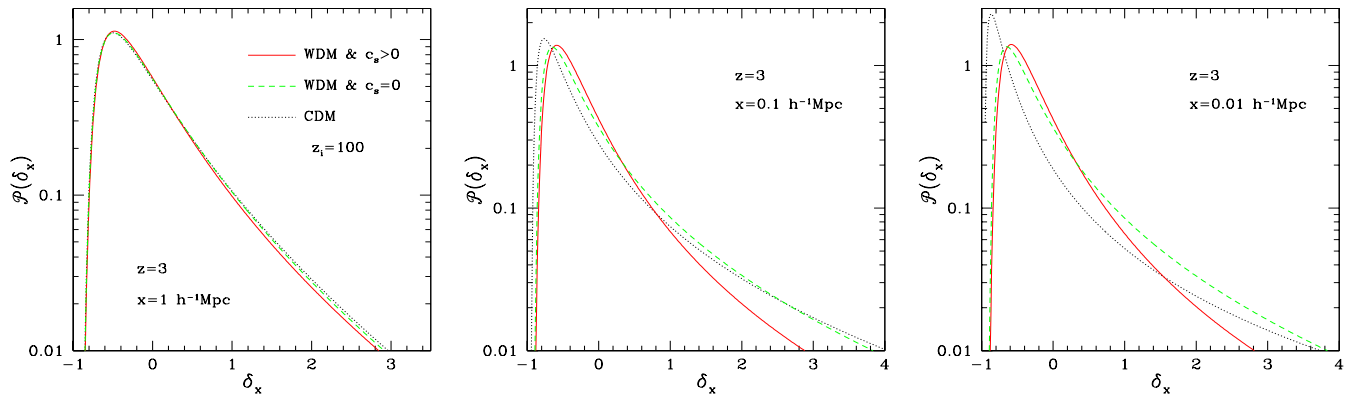


FIG. 5: Probability distribution $\mathcal{P}(\delta_x)$ of the matter density contrast within spheres of radius x , for three radii. We show our results at $z = 3$ for the reference CDM scenario (black dotted lines), the WDM scenarios with $c_s = 0$ (green dashed lines), and with $c_s \neq 0$ (red solid lines).

estimated the WDM halo mass function in the excursion-set formalism. These authors also find that the effect of the velocity dispersion, if it is estimated from its impact on the critical overdensity, is very small on the relevant mass scales (so that the cutoff of the halo mass function at low mass is set by the initial cutoff of the power spectrum (16)). However, they find that if one modifies in addition the scaling function $f(\nu)$, to take into account the dependence of the mass function on the global shape of the function $\delta_c(M)$ (and not only on its value at the mass M of interest), the low-mass cutoff becomes sharper. This second effect is not included in our paper (it requires additional modeling, such as the excursion set formalism, which needs to be checked against numerical simulations in this regime).

C. Probability distribution of the density contrast

Finally, we consider the probability distribution $\mathcal{P}(\delta_x)$ of the density contrast within spheres of radius x . As in [55], we use a steepest-descent approach to obtain $\mathcal{P}(\delta_x)$ from the spherical dynamics [63, 66]. This is valid in the mildly nonlinear regime. We plot our results in Fig. 5 at $z = 3$, on scales that correspond to Lyman- α clouds. Indeed, depending on the details of the models Lyman- α clouds are associated with scales from $\sim 10h^{-1}\text{kpc}$ to $\sim 1h^{-1}\text{Mpc}$ (from the small Lyman- α forest clouds to damped systems) [67–69].

We recover the characteristic asymmetry induced by the nonlinear gravitational dynamics, with a shift of the peak toward underdensities (most of the volume is underdense), a very sharp low-density cutoff ($\delta_x \geq -1$ since the matter density is always positive), and an extended high-density tail (most of the mass is within overdensities). On large scales, $x \geq 1h^{-1}\text{Mpc}$, all curves are very close and the deviations between the CDM and WDM scenarios are small. On smaller scales, the lack of small-scale power in

the WDM scenario leads to a less advanced stage of the nonlinear evolution: the peak shifts closer to the mean $\langle \delta_x \rangle = 0$, and the tails are sharper. The late-time velocity dispersion even further impedes the nonlinear evolution and makes the large density tail sharper. This suggests that accurate measures of the probability distribution of the flux decrement of distant quasars, due to Lyman- α absorption lines, which is closely related to the probability distribution of the matter density on these scales [67, 70], could be sensitive to this late-time velocity dispersion. Thus, numerical simulations that do not include this effect are likely to underestimate somewhat the difference between the CDM and WDM scenarios with respect to Lyman- α absorption lines.

It is not surprising that these statistics are more sensitive to the late-time velocity dispersion than the quantities studied in previous figures (the power spectrum on large perturbative scales and the halo mass function). Indeed, it is well-known that, because they probe relatively small scales, Lyman- α clouds are a sensitive probe of WDM scenarios. Most works focus on the decrease of the flux power spectrum due to the high- k damping of the WDM power spectrum set by the relativistic free streaming [18–20]. Figure 5 shows that the late-time velocity dispersion also has a non-negligible effect.

D. Range of validity of our approximations

Here we briefly comment on the validity of our method for the results described in the previous sections. Two effects are not fully included in our treatment of the dynamics:

- nonlinearities beyond one-loop order for the computation of the power spectrum,
- effects associated with the velocity dispersion that go beyond an effective pressure.

The errors associated with a) can be estimated in Fig. 2

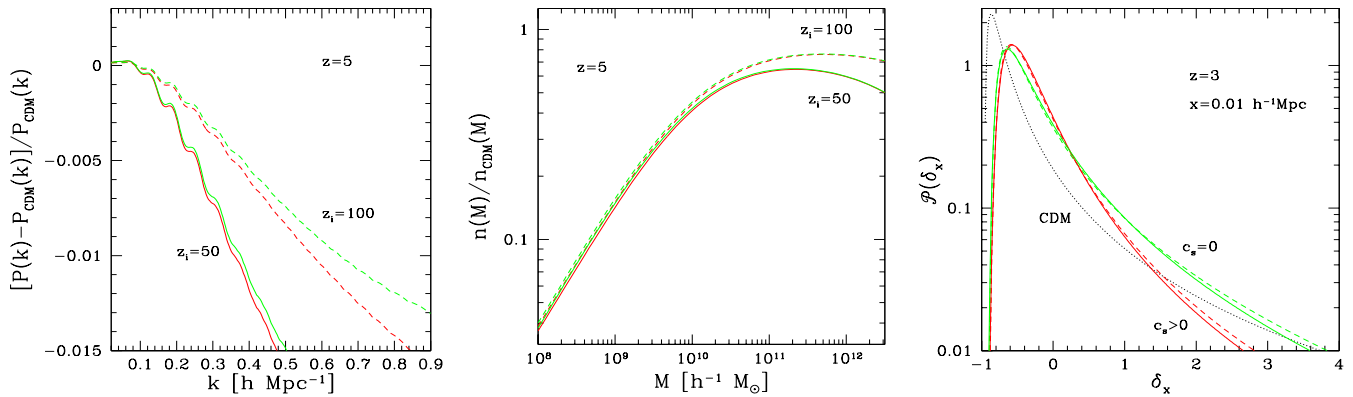


FIG. 6: *Left panel*: relative deviation of the power spectrum from the CDM reference, as in Fig. 3, using an initial redshift $z_i = 50$ (solid lines) or $z_i = 100$ (dashed lines). *Middle panel*: ratio of the WDM halo mass function to the CDM halo mass function, with $z_i = 50$ (solid lines) or $z_i = 100$ (dashed lines). *Right panel*: probability distribution of the matter density contrast, as in Fig. 5, for the CDM case, and for the WDM case with $z_i = 50$ (solid lines) and $z_i = 100$ (dashed lines). In each panel, the green curves (which correspond to slightly higher $P(k)$ and higher $\mathcal{P}(\delta_x)$ at $\delta_x > 2$) are obtained for $c_s = 0$ and the lower red curves are for $c_s \neq 0$.

by the comparison between the standard perturbation theory and the resummation scheme. Even though the latter is systematically more accurate, the difference between the two results gives an estimate of the error of the theoretical predictions on these scales. Then, as already noticed, one can safely conclude that, in this regime, the effect of the late-time velocity dispersion is on the order or smaller than the accuracy of standard perturbation theory.

The errors associated with b) can be estimated from the difference between the cases $c_s = 0$ and $c_s > 0$. As explained in Sec. II A, at late times, the main effect of the velocity dispersion should be well described by the “pressure” term in Eqs.(4) and (9). Then, as long as the deviation between the two cases $c_s = 0$ and $c_s > 0$ is small, one expects that we obtain the correct order of magnitude. In the regime where the deviation would be large (at very high redshift), higher-order corrections are expected to come into play. Therefore, our method should be sufficient for our purposes, in the regimes studied here[77].

IV. IMPACT OF LOWER INITIAL REDSHIFT

In the previous figures, we set the initial conditions at redshift $z_i = 100$. In this section, we investigate the impact of using a lower initial redshift, $z_i = 50$. This should make the two WDM results, with $c_s = 0$ and $c_s \neq 0$, closer to each other, since the velocity dispersion decreases with time. However, because it also sets the nonlinear contributions to zero at $z_i = 50$ instead of $z_i = 100$, this also further underestimates gravitational clustering.

In the standard Λ CDM scenario, we usually take the

limit $z_i \rightarrow \infty$ within analytical approaches because one is only interested in accurate predictions [61, 71, 72]. Moreover, numerical simulations often use second-order Lagrangian perturbation theory for their initial conditions to decrease the sensitivity to the initial redshift [73]. However, WDM simulations often use linear theory to set up their initial conditions. Indeed, a second-order implementation should, in principle, make use of a second-order analysis of the Vlasov equation at early times, while most works use the results obtained from the linearized Vlasov equation. On the other hand, the choice of the initial redshift is not so obvious in WDM scenarios, because a high initial redshift z_i can lead to spurious effects due to inadequate modeling of the large velocity dispersion [52], whereas a low initial redshift alleviates this problem but can lead to an underestimate of gravitational clustering.

The dependence on the initial redshift z_i is easily included within our analytic approach as follows. In the perturbative framework, used for the large-scale power spectrum shown in Figs. 1-2, the integrals over time associated with the one-loop and higher-order contributions run from z_i down to the redshift z of interest. In the spherical dynamics, used for the mass function and the density probability distribution shown in Figs. 4 and 5, the equations of motion are also integrated from the initial redshift z_i . This allows us to obtain the dependence on z_i of the large-scale structures built at a given redshift z , as in numerical simulations initialized at linear order at this redshift z_i . We show our results for the density power spectrum, the halo mass function, and the density probability distribution function, comparing the choices $z_i = 50$ and $z_i = 100$, in Fig. 6[78].

The left panel shows that on perturbative scales, $k < 0.9 h \text{Mpc}^{-1}$ at $z = 5$, using an initial redshift of $z_i = 50$

leads to an underestimation of the power spectrum on the order of 1%. Moreover, this is larger than the decrease of the power spectrum due to the change from the CDM to the WDM power spectrum. On the other hand, the difference between the $c_s = 0$ and $c_s \neq 0$ results is very small. The same behavior is found for the halo mass function, as shown by the middle panel, with an underestimation of the large-mass tail because of the low initialization redshift z_i that is on the order of or larger than the true decrease due to the WDM scenario. The low-mass tail is less affected by the value of the initial redshift since it corresponds to moderate density fluctuations. In contrast, the large-mass tail corresponds to rare events, which amplifies the sensitivity to the initial conditions. This also explains why we find in the right panel that using a low initial redshift $z_i = 50$ does not significantly change the probability distribution of the density contrast at $z = 3$, for moderate density fluctuations. Moreover, the difference between the $c_s = 0$ and $c_s \neq 0$ results remains similar to the one obtained with $z_i = 100$. Therefore, starting at $z_i = 50$ instead of $z_i = 100$ degrades the accuracy of measures of gravitational clustering at low redshifts, since it significantly underestimates the nonlinearities (as measured by the large-scale power spectrum or the halo mass function) and contaminates the signal associated with the WDM high- k cutoff (on large perturbative scales or on the large-mass tail of the halo mass function). Moreover, using $z_i = 50$ does not help to reduce the effect of the late-time velocity dispersion on the shape of $\mathcal{P}(\delta_x)$ on Lyman- α scales. Thus, numerical simulations should use a high initial redshift, $z_i \geq 100$, rather than a low value, $z_i \leq 50$.

V. CONCLUSION

Using an effective Euler equation, that agrees with the Vlasov equation at the linear level (except for subdominant memory terms), we have estimated the impact of a late-time WDM velocity dispersion on the formation of large-scale structures. We have only considered the “cosmic web”, that is, large perturbative scales, moderate density fluctuations, and the number counts of virialized halos, which can be studied with analytic tools. We have focused on the case of a 1keV dark matter particle, which is representative of current WDM scenarios (lower masses are excluded by observations, such as Lyman- α forest data, while higher masses become indistinguishable from the CDM limit).

We find that on perturbative scales, the deviation of the density power spectrum from the CDM case is only

on the order of 1%, at $z \leq 5$, even though it is slightly amplified by the nonlinear dynamics. This is below the accuracy of the standard perturbative expansion and requires efficient perturbative schemes. On the other hand, the effects of the late-time velocity dispersion are negligible over most of the perturbative range at $z \leq 5$ (so that one could use the same perturbative approaches devised for the CDM case). We also find that the late-time velocity dispersion has a negligible impact on the halo mass function at $z \leq 5$ (in any case, below the 10% accuracy that can be guaranteed by simulations), although at very low mass and high redshift, the cutoff may become sharper [64, 65]. On the other hand, it has a non-negligible effect on the probability distribution of the density contrast on scales $x \leq 0.1h^{-1}\text{Mpc}$ at $z = 3$. This means it should have some impact on the probability distribution of the Lyman- α flux decrement, measured on the spectra of distant quasars.

Finally, we note that numerical simulations should use a high initial redshift, $z_i \geq 100$, rather than a low value, $z_i \leq 50$. Indeed, such a low initial redshift can lead to a significant underestimation of the power spectrum on perturbative scales and of the large-mass tail of the halo mass function, which is larger than the true signal associated with the WDM scenario (but of course, on smaller scales and on the low mass tail of the mass function, one is again dominated by the actual WDM signal). A low initial redshift does not help much either to reduce the effect of the late-time velocity dispersion for the probability distribution of the density contrast on scales associated with Lyman- α clouds.

To go beyond the effective hydrodynamical equations used in this work, one should use the nonlinear Vlasov equation itself. However, this is a difficult task because of the additional velocity coordinates, which makes numerical implementations significantly heavier already for the CDM scenario [74, 75]. An alternative would be to extend the fluid approximation to higher orders [50], by including equations of motion for the velocity moments of the Vlasov equation up to some higher order $n \geq 3$. However, because most of the WDM signal arises from nonperturbative scales, such a task may not be very rewarding, unless one builds methods that can be applied to the Lyman- α forest clouds, for instance.

Acknowledgments

This work was performed using HPC resources from GENCI-CCRT (Grant 2012-t2012046803).

-
- [1] P. J. E. Peebles, *The large-scale structure of the universe* (Princeton University Press, Princeton, N.J., USA, 1980).
- [2] E. Komatsu, K. M. Smith, J. Dunkley, C. L. Bennett,

- B. Gold, G. Hinshaw, N. Jarosik, D. Larson, M. R.olta, L. Page, et al., *Astrophys. J. Suppl. Ser.* **192**, 18 (2011), 1001.4538.
- [3] M. Tegmark, D. J. Eisenstein, M. A. Strauss, D. H. Wein-

- berg, M. R. Blanton, J. A. Frieman, M. Fukugita, J. E. Gunn, A. J. S. Hamilton, G. R. Knapp, et al., *Phys. Rev. D* **74**, 123507 (2006), arXiv:astro-ph/0608632.
- [4] B. Moore, S. Ghigna, F. Governato, G. Lake, T. Quinn, J. Stadel, and P. Tozzi, *Astrophys. J. Letter* **524**, L19 (1999), arXiv:astro-ph/9907411.
- [5] V. Springel, J. Wang, M. Vogelsberger, A. Ludlow, A. Jenkins, A. Helmi, J. F. Navarro, C. S. Frenk, and S. D. M. White, *Mon. Not. R. Astron. Soc.* **391**, 1685 (2008), 0809.0898.
- [6] S. Trujillo-Gomez, A. Klypin, J. Primack, and A. J. Romanowsky, *Astrophys. J.* **742**, 16 (2011), 1005.1289.
- [7] J. F. Navarro, C. S. Frenk, and S. D. M. White, *Astrophys. J.* **490**, 493 (1997), arXiv:astro-ph/9611107.
- [8] A. Burkert, *Astrophys. J. Letter* **447**, L25 (1995), arXiv:astro-ph/9504041.
- [9] P. Salucci and A. Burkert, *Astrophys. J. Letter* **537**, L9 (2000), arXiv:astro-ph/0004397.
- [10] W. J. G. de Blok, *Advances in Astronomy* **2010**, 789293 (2010), 0910.3538.
- [11] P. Bode, J. P. Ostriker, and N. Turok, *Astrophys. J.* **556**, 93 (2001), arXiv:astro-ph/0010389.
- [12] V. Avila-Reese, P. Colín, O. Valenzuela, E. D’Onghia, and C. Firmani, *Astrophys. J.* **559**, 516 (2001), arXiv:astro-ph/0010525.
- [13] N. Menci, F. Fiore, and A. Lamastra, *Mon. Not. R. Astron. Soc.* **421**, 2384 (2012), 1201.1617.
- [14] M. R. Lovell, V. Eke, C. S. Frenk, L. Gao, A. Jenkins, T. Theuns, J. Wang, S. D. M. White, A. Boyarsky, and O. Ruchayskiy, *Mon. Not. R. Astron. Soc.* **420**, 2318 (2012), 1104.2929.
- [15] H. J. de Vega and N. G. Sanchez, *Mon. Not. R. Astron. Soc.* **404**, 885 (2010), 0901.0922.
- [16] H. J. de Vega, P. Salucci, and N. G. Sanchez, *New Astronomy* **17**, 653 (2012).
- [17] J. E. Gunn and B. A. Peterson, *Astrophys. J.* **142**, 1633 (1965).
- [18] M. Viel, J. Lesgourgues, M. G. Haehnelt, S. Matarrese, and A. Riotto, *Phys. Rev. D* **71**, 063534 (2005), arXiv:astro-ph/0501562.
- [19] U. Seljak, A. Makarov, P. McDonald, and H. Trac, *Physical Review Letters* **97**, 191303 (2006), arXiv:astro-ph/0602430.
- [20] K. Abazajian, *Phys. Rev. D* **73**, 063513 (2006), arXiv:astro-ph/0512631.
- [21] A. Boyarsky, J. Lesgourgues, O. Ruchayskiy, and M. Viel, *Physical Review Letters* **102**, 201304 (2009), 0812.3256.
- [22] J. S. Bullock, A. V. Kravtsov, and D. H. Weinberg, *Astrophys. J.* **539**, 517 (2000), arXiv:astro-ph/0002214.
- [23] A. J. Benson, C. S. Frenk, C. G. Lacey, C. M. Baugh, and S. Cole, *Mon. Not. R. Astron. Soc.* **333**, 177 (2002), arXiv:astro-ph/0108218.
- [24] G. Kauffmann, S. D. M. White, and B. Guiderdoni, *Mon. Not. R. Astron. Soc.* **264**, 201 (1993).
- [25] S. Kopolov, V. Belokurov, N. W. Evans, P. C. Hewett, M. J. Irwin, G. Gilmore, D. B. Zucker, H.-W. Rix, M. Fellhauer, E. F. Bell, et al., *Astrophys. J.* **686**, 279 (2008), 0706.2687.
- [26] S. Mashchenko, H. M. P. Couchman, and J. Wadsley, *Nature (London)* **442**, 539 (2006), arXiv:astro-ph/0605672.
- [27] F. Governato, C. Brook, L. Mayer, A. Brooks, G. Rhee, J. Wadsley, P. Jonsson, B. Willman, G. Stinson, T. Quinn, et al., *Nature (London)* **463**, 203 (2010).
- [28] R. S. de Souza, L. F. S. Rodrigues, E. E. O. Ishida, and R. Opher, *Mon. Not. R. Astron. Soc.* **415**, 2969 (2011), 1104.2850.
- [29] A. S. Font, A. J. Benson, R. G. Bower, C. S. Frenk, A. Cooper, G. De Lucia, J. C. Helly, A. Helmi, Y.-S. Li, I. G. McCarthy, et al., *Mon. Not. R. Astron. Soc.* **417**, 1260 (2011), 1103.0024.
- [30] S. Dodelson and L. M. Widrow, *Physical Review Letters* **72**, 17 (1994), arXiv:hep-ph/9303287.
- [31] K. Abazajian, G. M. Fuller, and M. Patel, *Phys. Rev. D* **64**, 023501 (2001), arXiv:astro-ph/0101524.
- [32] K. Abazajian and S. M. Koushiappas, *Phys. Rev. D* **74**, 023527 (2006), arXiv:astro-ph/0605271.
- [33] M. Shaposhnikov and I. Tkachev, *Physics Letters B* **639**, 414 (2006), arXiv:hep-ph/0604236.
- [34] A. Boyarsky, O. Ruchayskiy, and M. Shaposhnikov, *Annual Review of Nuclear and Particle Science* **59**, 191 (2009), 0901.0011.
- [35] A. Kusenko, *Phys. Rep.* **481**, 1 (2009), 0906.2968.
- [36] K. N. Abazajian, M. A. Acero, S. K. Agarwalla, A. A. Aguilar-Arevalo, C. H. Albright, S. Antusch, C. A. Argüelles, A. B. Balantekin, G. Barenboim, V. Barger, et al., *ArXiv e-prints* (2012), 1204.5379.
- [37] M. Kawasaki, N. Sugiyama, and T. Yanagida, *Modern Physics Letters A* **12**, 1275 (1997), arXiv:hep-ph/9607273.
- [38] D. Gorbunov, A. Khmelnskiy, and V. Rubakov, *Journal of High Energy Physics* **12**, 55 (2008), 0805.2836.
- [39] D. Boyanovsky, H. J. de Vega, and N. G. Sanchez, *Phys. Rev. D* **78**, 063546 (2008), 0807.0622.
- [40] D. Boyanovsky and J. Wu, *Phys. Rev. D* **83**, 043524 (2011), 1008.0992.
- [41] D. Boyanovsky, *Phys. Rev. D* **83**, 103504 (2011), 1011.2217.
- [42] H. J. de Vega and N. G. Sanchez, *Phys. Rev. D* **85**, 043516 (2012), 1111.0290.
- [43] H. J. de Vega and N. G. Sanchez, *Phys. Rev. D* **85**, 043517 (2012), 1111.0300.
- [44] A. Schneider, R. E. Smith, A. V. Maccio, and B. Moore, *ArXiv e-prints* (2011), 1112.0330.
- [45] R. E. Smith and K. Markovic, *Phys. Rev. D* **84**, 063507 (2011), 1103.2134.
- [46] R. M. Dunstan, K. N. Abazajian, E. Polisensky, and M. Ricotti, *ArXiv e-prints* (2011), 1109.6291.
- [47] S. Tremaine and J. E. Gunn, *Physical Review Letters* **42**, 407 (1979).
- [48] C. J. Hogan and J. J. Dalcanton, *Phys. Rev. D* **62**, 063511 (2000), arXiv:astro-ph/0002330.
- [49] J. Viñas, E. Salvador-Solé, and A. Manrique, *Mon. Not. R. Astron. Soc.* **424**, L6 (2012), 1202.2860.
- [50] M. Shoji and E. Komatsu, *Phys. Rev. D* **81**, 123516 (2010).
- [51] S. Colombi, S. Dodelson, and L. M. Widrow, *Astrophys. J.* **458**, 1 (1996), arXiv:astro-ph/9505029.
- [52] P. Colín, O. Valenzuela, and V. Avila-Reese, *Astrophys. J.* **673**, 203 (2008), 0709.4027.
- [53] A. Boyarsky, J. Lesgourgues, O. Ruchayskiy, and M. Viel, *JCAP* **5**, 12 (2009), 0812.0010.
- [54] M. Viel, K. Marković, M. Baldi, and J. Weller, *Mon. Not. R. Astron. Soc.* **421**, 50 (2012), 1107.4094.
- [55] P. Brax and P. Valageas, *ArXiv e-prints* (2012), 1205.6583.
- [56] A. V. Maccio’, S. Paduroiu, D. Anderhalden, A. Schneider, and B. Moore, *ArXiv e-prints* (2012), 1202.1282.

- [57] D. J. Eisenstein, W. Hu, and M. Tegmark, *Astrophys. J.* **518**, 2 (1999), arXiv:astro-ph/9807130.
- [58] F. Bernardeau, S. Colombi, E. Gaztañaga, and R. Scoccimarro, *Phys. Rep.* **367**, 1 (2002), arXiv:astro-ph/0112551.
- [59] P. Valageas, *Astron. & Astrophys.* **465**, 725 (2007), arXiv:astro-ph/0611849.
- [60] P. Valageas, *Astron. & Astrophys.* **484**, 79 (2008), 0711.3407.
- [61] P. Valageas and T. Nishimichi, *Astron. & Astrophys.* **527**, A87+ (2011), 1009.0597.
- [62] W. H. Press and P. Schechter, *Astrophys. J.* **187**, 425 (1974).
- [63] P. Valageas, *Astron. & Astrophys.* **508**, 93 (2009), 0905.2277.
- [64] R. Barkana, Z. Haiman, and J. P. Ostriker, *Astrophys. J.* **558**, 482 (2001), arXiv:astro-ph/0102304.
- [65] A. J. Benson, A. Farahi, S. Cole, L. A. Moustakas, A. Jenkins, M. Lovell, R. Kennedy, J. Helly, and C. Frenk, *Mon. Not. R. Astron. Soc.* (2012), 1209.3018.
- [66] P. Valageas, *Astron. & Astrophys.* **382**, 412 (2002), arXiv:astro-ph/0107126.
- [67] P. Valageas, R. Schaeffer, and J. Silk, *Astron. & Astrophys.* **345**, 691 (1999), arXiv:astro-ph/9903388.
- [68] H. Bi, *Astrophys. J.* **405**, 479 (1993).
- [69] M. J. Rees, *Mon. Not. R. Astron. Soc.* **218**, 25P (1986).
- [70] M. Viel, S. Matarrese, H. J. Mo, T. Theuns, and M. G. Haehnelt, *Mon. Not. R. Astron. Soc.* **336**, 685 (2002), arXiv:astro-ph/0203418.
- [71] P. Valageas and T. Nishimichi, *Astron. & Astrophys.* **532**, A4+ (2011), 1102.0641.
- [72] P. Valageas, M. Sato, and T. Nishimichi, arXiv:1111.7156 (paper I) (2011), 1111.7156.
- [73] R. Scoccimarro, *Mon. Not. R. Astron. Soc.* **299**, 1097 (1998), arXiv:astro-ph/9711187.
- [74] P. Valageas, *Astron. & Astrophys.* **421**, 23 (2004), arXiv:astro-ph/0307008.
- [75] S. V. Tassev, *JCAP* **10**, 22 (2011), 1012.0282.
- [76] To avoid spending most of the computation time on high k wavenumbers where the initial power is very small, as seen in Fig. 1, we set a lower bound $\epsilon(k, \tau) \geq -0.5$ in the numerical computations.
- [77] It is not possible to compare with current simulations because they do not include the effect of the velocity dispersion (apart from the definition of the initial conditions) and our simple approach with this effective pressure term is already beyond what is done in simulations. (The same algorithms are used for CDM and WDM in N-body codes.)
- [78] We choose these two values because they are commonly used in numerical simulations. Moreover, considering high values such as $z_i = 1000$ would not be so useful because simulations avoid such high initial redshifts to save computational time and to avoid the regime where the impact of velocity dispersion is large (which is not included in a rigorous manner in N-body codes).